Density-Functional-Theory Studies of the Infrared Spectra of Titanium Carbide Nanocrystals

Michael Patzschke and Dage Sundholm*

Department of Chemistry, University of Helsinki, P.O. Box 55 A.I. Virtanens plats 1, FIN-00014 Helsinki, Finland

Received: October 26, 2004; In Final Form: March 21, 2005

The infrared (IR) spectra of cuboidic titanium carbide (TiC) nanocrystals have been studied at the density-functional-theory (DFT) level using the Becke−Perdew (BP) functional and triple-ζ quality basis sets augmented by one set of polarization functions (TZVP). The accuracy of the calculations was checked by DFT calculations using the Perdew−Burke−Ernzerhof hybrid functional (PBE0) and up to quadruple-ζ quality basis sets augmented by one set of polarization functions (QZVP). The calculated IR spectrum for $Ti_{14}C_{13}$ ($3 \times 3 \times 3$) is found to be in fair agreement with the experimental IR spectrum obtained by infrared resonance-enhanced multiphoton ionization (IR-REMPI) measurements, whereas, for $Ti_{18}C_{18}$ ($4 \times 3 \times 3$) and $Ti_{32}C_{32}$ ($4 \times 4 \times 4$), the calculated IR spectra differ significantly from the experimental ones. The smallest TiC cluster (Ti_4C_4, $2 \times 2 \times 2$) considered has not been reported in any mass-spectrometer studies. The present DFT calculations show that the vibrational modes related to the in-plane vibrations of solid TiC are not observed in the IR-REMPI spectra of nanocrystals larger than $Ti_{14}C_{13}$. Contrary to solid TiC, the studied TiC nanocrystals are nonmetallic with optical gaps of 0.62 eV (0.55 eV) and 0.028 eV (0.027 eV) for $Ti_{32}C_{32}$ and $Ti_{108}C_{108}$ ($6 \times 6 \times 6$), calculated at the time-dependent density-functional-theory (TDDFT) level using the BP functional. The HOMO−LUMO gaps obtained in the BP DFT calculations are given within parentheses. At the PBE0 DFT level, the HOMO−LUMO gaps for $Ti_{32}C_{32}$ and $Ti_{108}C_{108}$ are 1.74 and 0.32 eV, respectively.

I. Introduction

The detection of the first metallocarbohedrene, Ti_8C_{12}, was reported by Guo et al. in 1992,[1] and the next year, Pilgrim and Duncan[2] reported observations of titanium−carbon species with cubic lattice structures obtained in similar laser vaporization experiments. Because of the cluster structure, Pilgrim and Duncan designated them as titanium carbide (TiC) nanocrystals.[2] The identification of the TiC nanoclusters relied on mass spectra showing strong peaks at cluster masses corresponding to face-centered-cuboidic structures with $N_x \times N_y \times N_z$ atoms (Ti or C) in the three Cartesian directions exhibiting a stoichiometric ratio of 1:1 for Ti/C. Pilgrim and Duncan[2] reported observations of perfect and truncated TiC nanocrystals such as $Ti_{18}C_{18}$ ($4 \times 3 \times 3$), $Ti_{23}C_{22}$ ($5 \times 3 \times 3$), $Ti_{24}C_{24}$ ($4 \times 4 \times 3$), $Ti_{27}C_{27}$ ($6 \times 3 \times 3$), $Ti_{30}C_{30}$ ($5 \times 4 \times 3$), $Ti_{32}C_{32}$ ($4 \times 4 \times 4$), and $Ti_{36}C_{36}$ ($6 \times 4 \times 3$). The existence of these cluster species in molecular beams have been verified by Helden et al.[3] who also detected larger TiC nanocrystals such as $Ti_{40}C_{40}$ ($5 \times 4 \times 4$), $Ti_{50}C_{50}$ ($5 \times 5 \times 4$), and $Ti_{63}C_{62}$ ($5 \times 5 \times 5$). For a review of various transition-metal carbenes, see ref 4.

Larger TiC nanocrystals have been proven to exhibit stoichiometric ratios deviating slightly from the expected 1:1. Experimental and computational studies have indicated that the bonds to carbon atoms in the corners of transition-metal carbide nanoclusters are much weaker than those for corner titanium atoms;[5] no perfect crystal fragments with corner carbons have yet been observed.[6] For example, $Ti_{13}C_{14}$ has not been detected in any mass-spectrometer measurements, whereas peaks corresponding to $Ti_{14}C_{13}$ and $Ti_{13}C_6$ have been found. The $Ti_{14}C_{13}$ nanocluster has a cubic ($3 \times 3 \times 3$) NaCl crystal structure with Ti atoms in all eight corners, whereas $Ti_{13}C_6$ corresponds to a truncated $3 \times 3 \times 3$ nanocrystal having a titanium atom at the crystallite center and lacking corner carbons.[2,5] More generally, transition-metal carbide nanocrystals with even N_x, N_y, or N_z seem to lack corner carbons. This conclusion has been drawn from mass spectra of vanadium carbide nanocrystals. Since the mass of the ^{48}Ti isotope and the mass of four carbon atoms coincide, a detailed interpretation of the mass spectra for a mixture of TiC nanocrystals is very difficult.[6] A recent density-functional-theory (DFT) study has also shown that carbon corner sites are energetically disfavored in transition-metal carbide nanocrystals.[5]

The mass spectrometry provided the molecular masses of the clusters, and a newly developed experimental technique to measure the IR spectra yielded vibrational information about the nanoclusters. The infrared resonance-enhanced multiphoton ionization (IR-REMPI) method has been applied on TiC nanocrystals and related species in molecular beams.[3,6−10] Also, other experimental techniques have been used to measure the vibrational (IR) spectra of nanoclusters.[11] The IR-REMPI spectrum provides low-resolution information about the vibrational spectra of the clusters in the beam. For example, it reveals whether any C−C bonds are present in the cluster but only a few bands corresponding to other vibrations can be resolved. IR-REMPI spectroscopy does not yield any detailed fingerprint information about the vibrations as traditional IR spectroscopy does. Thus, it is rather complicated to extract structural information from the measured IR-REMPI spectra. IR-REMPI studies of C_{60} have shown that the peaks of the IR-REMPI spectrum are slightly red shifted as compared to ordinary IR spectra.[3] Few other techniques to measure IR spectra of TiC nanoclusters have been successful.[11] However, nowadays, first-principle computational methods with a rather high accuracy can be used to obtain IR spectra of large nanocrystals and

10.1021/jp045126n CCC: $30.25 © 2005 American Chemical Society
Published on Web 06/02/2005

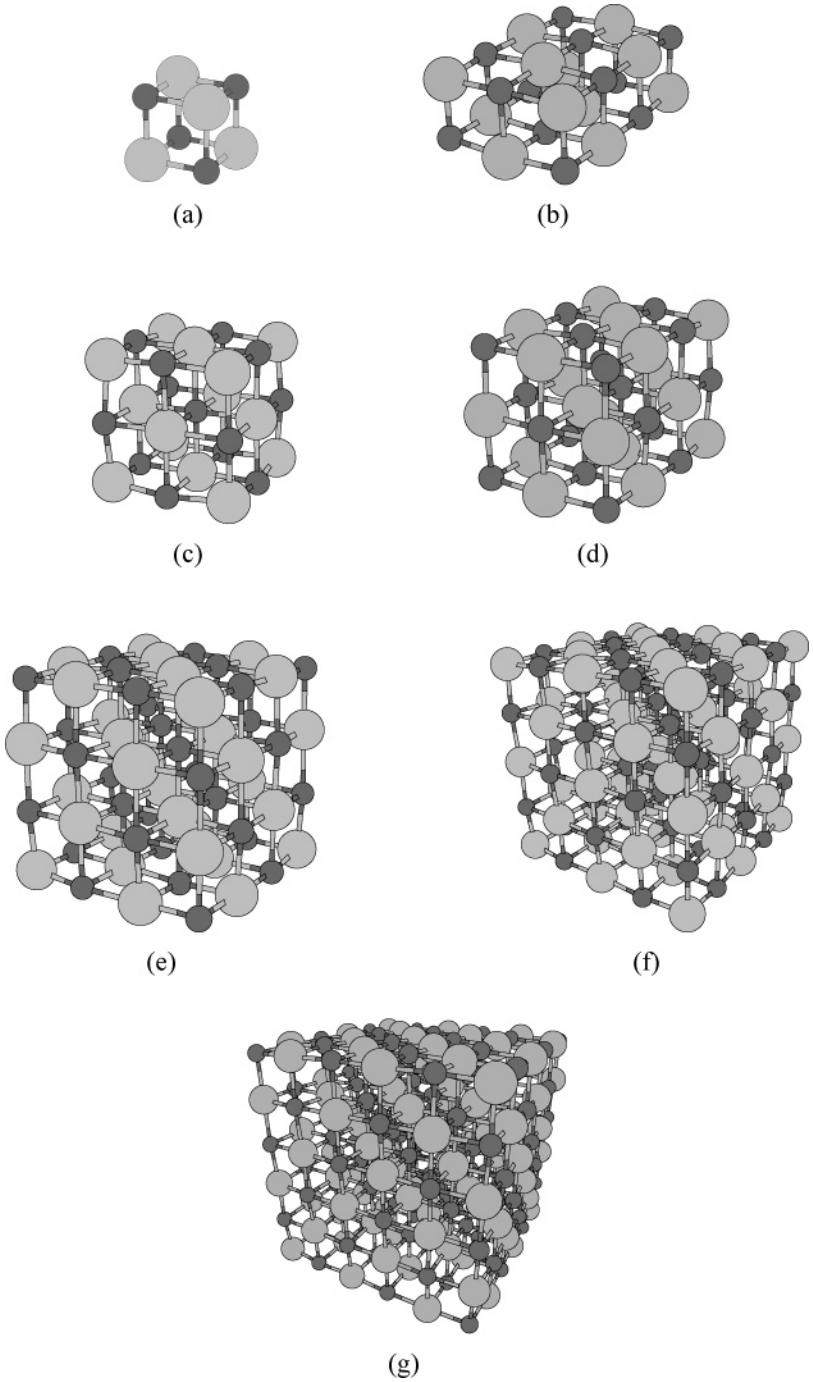

Figure 1. Molecular structure of (a) Ti_4C_4 ($2 \times 2 \times 2$), (b) $Ti_{12}C_{12}$ ($4 \times 3 \times 2$), (c) $Ti_{14}C_{13}$ ($3 \times 3 \times 3$), (d) $Ti_{18}C_{18}$ ($4 \times 3 \times 3$), and (e) $Ti_{32}C_{32}$ ($4 \times 4 \times 4$) calculated at the BP DFT/TZVP level. The molecular structures of (f) $Ti_{63}C_{62}$ ($5 \times 5 \times 5$) and (g) $Ti_{108}C_{108}$ ($6 \times 6 \times 6$) were optimized at the BP DFT/SVP level.

clusters. Comparisons of the calculated and measured IR spectra can facilitate the characterization of the nanoparticles present in the molecular beam. Such studies on metallocarbohedrenes, M_8C_{12}, have been recently reported.[12−16] In this work, we extend this kind of study to include experimentally reported TiC nanocrystals. The IR spectrum for $Ti_{14}C_{13}$ ($3 \times 3 \times 3$) has previously been calculated at the DFT level,[17] but to the best of our knowledge, the IR spectra of the larger nanocrystals have not been previously studied using first-principle computational methods.

The experimental IR-REMPI spectra of TiC nanocrystals are dominated by a strong resonance at 485 cm^{-1}, and the position of the peak is independent of the size of the cluster. For smaller TiC nanoclusters such as $Ti_{14}C_{13}$, another band appears at 600−700 cm^{-1}. Electron-energy-loss spectroscopy (EELS) measurements on solid TiC indicate that these two bands correspond to atomic motions perpendicular and parallel to the surface of bulk TiC.[3,19] For the larger clusters, the IR-REMPI intensity of the band at 600−700 cm^{-1} is weak, and for the largest clusters considered, it even disappears into the background noise. For very large TiC clusters, the experimental IR spectrum is expected to become broad and unstructured, since for them the transformation from molecular clusters with significant optical gaps into a conducting species with a small or no optical gap is expected to occur. For a cluster with an optical gap of the same size as the energy of the infrared radiation, the IR-REMPI experiment involves combined electronic and vibrational excitations.

Here, we calculate the vibrational spectra of TiC clusters in order to understand why the IR-REMPI spectra of the TiC clusters do not follow a continuous transformation from the one obtained for the smallest clusters to a spectrum corresponding to the vibrational levels of solid TiC. The energy gap between the highest occupied molecular orbital (HOMO) and the lowest unoccupied molecular orbital (LUMO) as well as the excitation energies of the first excited singlet states have also been studied at the DFT level. The largest species considered in this work are the $Ti_{63}C_{62}$ ($5 \times 5 \times 5$) and $Ti_{108}C_{108}$ ($6 \times 6 \times 6$) nanocrystals.

II. Computational Methods

The molecular structures of the TiC nanocrystals were fully optimized at the density-functional-theory (DFT) level[20] employing the Becke−Perdew (BP) generalized-gradient approximation (GGA) functional[21−23] as implemented in TURBOMOLE.[24] In the BP DFT calculations, the resolution of the identity (density fitting) approach was used to speed up the calculations.[20] The Karlsruhe triple-ζ valence quality basis sets augmented by one set of polarization functions (TZVP)[25,26] were used as the default basis set in this study. The vibrational frequencies were calculated numerically at the BP DFT level using the NUMFORCE module of TURBOMOLE.[24] The excitation energies were calculated at the time-dependent density-functional-theory (TDDFT) level using the BP functional.[27−29] For the smaller TiC clusters, the TZVP basis set was employed in the structural optimizations, in the calculations of the vibrational frequencies, and in the calculation of the optical gap, whereas the molecular structure calculations and the calculations of the optical gap of the largest nanocrystals, that is, $Ti_{63}C_{62}$ and $Ti_{108}C_{108}$, were performed using split-valence basis sets augmented with polarization functions (SVP).[30]

The accuracy of the BP DFT/TZVP calculations was checked by performing BP DFT calculations on Ti_4C_4 using the Karlsruhe triple-ζ basis sets augmented with double polarization functions (TZVPP) as well as the Karlsruhe quadruple-ζ basis sets augmented with one set of polarization functions (QZVP).[24] DFT calculations using the Perdew−Burke−Ernzerhof hybrid functional (PBE0)[31] were also employed in order to study the changes in the vibrational frequencies and HOMO−LUMO gaps due to exact Hartree−Fock exchange terms in the functional. The molecular structures were optimized at the PBE0 DFT/TZVP level for all clusters up to $Ti_{32}C_{32}$. The vibrational frequencies were studied at the PBE0 DFT/TZVP level for Ti_4C_4 and $Ti_{14}C_{13}$. The PBE0 DFT/SVP single-point calculations on $Ti_{63}C_{62}$ and $Ti_{108}C_{108}$ suffered from convergence problems.

III. Structures

The optimized structures of the TiC nanocrystals are displayed in Figure 1. The symmetries of the fully optimized Ti_4C_4, $Ti_{12}C_{12}$, $Ti_{14}C_{13}$, $Ti_{18}C_{18}$, $Ti_{32}C_{32}$, $Ti_{63}C_{62}$, and $Ti_{108}C_{108}$ nanocrystals were found to be T_d, C_{2h}, D_{2h}, C_{4v}, T_d, D_{2h}, and T_d, respectively. Since the cuboidic nanocrystals have a huge number of chemical bonds, their size and structure can most conveniently be represented by their volumes and bond-length distributions. The molecular volumes estimated from the distance between the corner atoms are 7.5, 64, 234, 565, and 1110 Å^3 for the $2 \times 2 \times 2$, $3 \times 3 \times 3$, $4 \times 4 \times 4$, $5 \times 5 \times 5$, and $6 \times 6 \times 6$ nanocrystals, respectively. The bond-length distribution for $Ti_{108}C_{108}$ calculated at the BP DFT/SVP level shown in Figure 2 may represent here all the nanocrystals considered. The Ti−C distances are in general somewhat shorter than the bulk value 216.37 pm.[32,33] The bonds at the crystallite center are the ones closest to the bulk Ti−C distance, whereas the shortest bond distances appear at the corners. The carbon atoms at the center of the crystallite surface are pushed out from the surface plane, yielding the longest Ti−C bonds of the $Ti_{108}C_{108}$ nanocrystal; the Ti−C distances perpendicular to the surface of the carbons at the center of the surface are 16 pm longer than those for the corresponding Ti atoms.

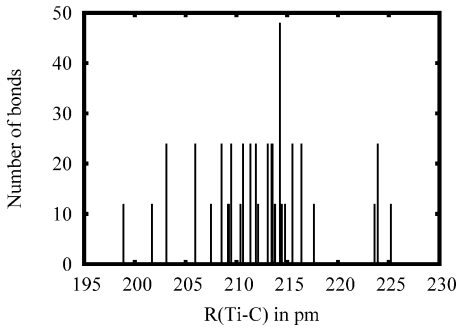

Figure 2. Bond-length distribution for $Ti_{108}C_{108}$ obtained at the BP DFT/SVP level.

TABLE 1: Longest and Shortest Ti−C Bond Lengths (in pm) for the TiC Nanoclusters Calculated at Different Levels of Theory (the HOMO−LUMO Gaps (H−L in eV) Are Also Given)

cluster	functional	basis set	*R*(Ti−C)	*R*(Ti−C)	H−L
Ti_4C_4	BP	TZVP	196.1	196.1	2.269
Ti_4C_4	PBE0	SVP	193.9	193.9	4.138
Ti_4C_4	PBE0	TZVP	194.1	194.1	4.096
Ti_4C_4	PBE0	TZVPP	193.7	193.7	4.147
Ti_4C_4	PBE0	QZVP	193.6	193.6	4.053
$Ti_{12}C_{12}$	BP	TZVP	190.0	219.6	1.010
$Ti_{12}C_{12}$	PBE0	TZVP	187.1	218.4	2.385
$Ti_{14}C_{13}$	BP	TZVP	201.0	216.5	0.060
$Ti_{14}C_{13}$	PBE0	TZVP	199.1	214.8	1.089
$Ti_{18}C_{18}$	BP	TZVP	195.1	222.5	0.416
$Ti_{18}C_{18}$	PBE0	TZVP	191.8	223.5	1.765
$Ti_{32}C_{32}$	BP	TZVP	198.2	220.0	0.547
$Ti_{32}C_{32}$	PBE0	TZVP	196.0	217.8	1.743
$Ti_{63}C_{62}$	BP	SVP	198.1	223.2	0.007
$Ti_{108}C_{108}$	BP	SVP	198.9	225.2	0.027
$Ti_{108}C_{108}$	PBE0	SVP			0.323[a]
TiC bulk			216.37[b]	216.37	0.0

[a] Single-point calculation using the BP DFT/TZVP structure. The calculation suffered from convergence problems. However, these problems probably did not affect the HOMO−LUMO gap significantly. [b] The lattice parameter of bulk TiC is 432.74 pm.[32,33]

The accuracy of the cluster structures optimized at the BP DFT/TZVP level was checked by performing a basis-set study on the Ti_4C_4 cluster. In the basis-set study, we employed larger basis sets of TZVPP and QZVP quality as well as the Karlsruhe SVP quality basis sets. The obtained bond distances are summarized in Table 1. In the basis-set study, the BP GGA and PBE0 hybrid functionals were employed. The basis-set study shows that the TZVP basis sets yield accurate cluster structures with TiC bond lengths that are only 0.5 pm longer than those obtained with the QZVP basis set. Thus, the molecular structures obtained using the TZVP basis sets are close to the BP DFT limit. The choice of the functional has a larger influence on the obtained bond distances. Differences in the bond distances of typically 2−3 pm were obtained in the calculations employing the BP GGA functional and the PBE0 hybrid functional, respectively.

IV. Vibrational Spectra

The vibrational energies of the Ti_4C_4 cluster calculated at the PBE0 DFT level using different basis sets are listed in Table

TABLE 2: Vibrational Energies of Ti_4C_4 (in cm^{-1}) Calculated at the PBE0 DFT Level Using SVP, TZVP, and TZVPP Quality Basis Sets

number	SVP	TZVP	TZVPP	QZVP
1	299	296	294	293
2[a]	373	368	364	360
3	472	463	460	458
4	485	487	485	491
5	524	525	520	522
6[a]	708	701	700	697
7	747	737	732	730
8[a]	773	764	766	769

[a] IR transitions with the nonzero intensities.

TABLE 3: Vibrational Energies (in cm^{-1}) of the Studied TiC Nanoclusters Calculated at the BP DFT/TZVP Level[a]

mode	Ti_4C_4	$Ti_{12}C_{12}$	$Ti_{14}C_{13}$	$Ti_{18}C_{18}$	$Ti_{32}C_{32}$	$Ti_{14}C_{13}$[b]
1	663^{m}	501^{vw}	275^{m}	278^{vw}	158^{vw}	223^{vw}
2	718^{m}	517^{w}	379^{vw}	311^{vw}	176^{vw}	272^{w}
3		529^{m}	486^{s}	501^{vw}	268^{vw}	274^{w}
4		553^{m}	514^{m}	506^{w}	354^{w}	483^{w}
5		620^{s}	515^{vw}	509^{vw}	448^{vw}	522^{vw}
6		658^{m}	555^{vw}	537^{s}	477^{vw}	523^{vw}
7		687^{s}	670^{vs}	591^{s}	533^{vs}	544^{s}
8		716^{m}	673^{s}	608^{m}	574^{w}	587^{vw}
9		733^{m}	713^{vw}	620^{s}	597^{vs}	711^{s}
10		743^{s}		704^{vw}	613^{m}	712^{s}
11		780^{w}		734^{s}	644^{w}	790^{w}
12				751^{w}	688^{vw}	
13				765^{m}	709^{vs}	
14				778^{s}	724^{m}	
15					737^{vw}	
16					753^{vw}	
omitted	1	22	10	30	10	14

[a] The intensities given as superscripts are denoted as follows: very weak (vw) transitions, that is, 20−50 km/mol; weak (w), 50−100 km/mol; medium (m), 100−200 km/mol; strong (s), 200−500 km/mol; very strong (vs) transitions have calculated intensities that are larger than 500 km/mol. Vibrational frequencies with intensities smaller than 20 km/mol are omitted. The number of omitted vibrational modes is given in the last row. [b] Calculated using the PBE0 hybrid functional.

2. The vibrational energies are almost independent of the size of the basis set used. The largest energy difference of 17 cm^{-1} between the vibrational energies calculated using the SVP and QZVP basis sets was obtained for the seventh vibrational transition in Table 2. The vibrational frequencies obtained in the PBE0 calculations are shifted to somewhat higher energies, since the molecular structures optimized using the PBE0 hybrid functional are more compact than the ones obtained in the BP DFT calculations. For Ti_4C_4, the vibrational frequencies calculated at the PBE0 DFT level are about 40 cm^{-1} larger than those obtained at the BP DFT level, whereas, for $Ti_{14}C_{13}$, the blue shifts are somewhat larger. The vibrational frequencies for $Ti_{14}C_{13}$ calculated at the PBE0 DFT/TZVP level are given in the last column of Table 3, and the corresponding IR spectra calculated at the PBE0 DFT/TZVP and BP DFT/TZVP levels are compared in Figure 3. The most important sources of the discrepancies between calculated vibrational frequencies and those obtained in the IR-REMPI experiment are the employed functional, anharmonicity effects, and experimental conditions of the IR-REMPI measurement such as the high cluster temperature and cooling pathways.

The IR spectra (in reciprocal centimeters) of the studied TiC nanocrystals calculated at the BP DFT/TZVP level are shown in Figure 4, and the numerical values for the harmonic vibrational frequencies are given in Table 3. Three strong peaks are obtained in the calculated IR spectrum for $Ti_{32}C_{32}$, which is the largest nanocrystal whose IR spectrum is calculated in

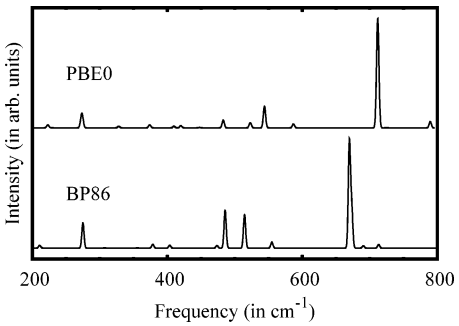

Figure 3. Comparison of the IR spectrum of $Ti_{14}C_{13}$ (in reciprocal centimeters) calculated at the BP DFT/TZVP and PBE0 DFT/TZVP levels of theory.

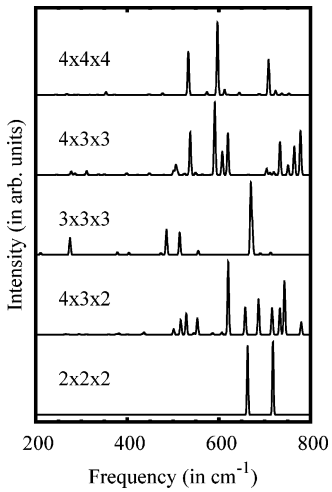

Figure 4. Infrared spectrum (in reciprocal centimeters) of Ti_4C_4 ($2 \times 2 \times 2$), $Ti_{12}C_{12}$ ($4 \times 3 \times 2$), $Ti_{14}C_{13}$ ($3 \times 3 \times 3$), $Ti_{18}C_{18}$ ($4 \times 3 \times 3$), and $Ti_{32}C_{32}$ ($4 \times 4 \times 4$) calculated at the BP DFT/TZVP level.

this work. The wavenumbers of these modes are 533, 597, and 709 cm^{-1}, respectively. In the calculated IR spectra of the smaller nanocrystals, also three strong transition bands are seen. Ti_4C_4 has three vibrational modes with nonzero intensities of which the lowest one at 351 cm^{-1} is a very weak transition and can hardly be detected in any experiment. The strongest IR transitions for $Ti_{12}C_{12}$ are obtained at 620, 687, and 743 cm^{-1}. $Ti_{14}C_{13}$ has four strong transitions at 275, 486, 670, and 673 cm^{-1}, yielding three strong IR bands. $Ti_{18}C_{18}$ has five strong transitions at 537, 591, 620, 734, and 778 cm^{-1}, also forming three IR bands. DFT calculations of the vibrational spectra of $Ti_{63}C_{62}$ and $Ti_{108}C_{108}$ would require a huge amount of computational resources and are therefore omitted.

For comparison, the measured IR-REMPI spectra of a few TiC nanocrystals are shown in Figure 5.[3] The IR-REMPI spectra of TiC nanocrystals are dominated by a strong resonance at 485 cm^{-1}. The position of this peak is found to be independent of the size of the nanocrystal and has been suggested to correspond to the motions perpendicular to the surface of the atoms in bulk TiC.[3] This interpretation was based on the fact that the positions of the two optically active phonon modes of the TiC(100) surface measured by electron-energy-loss spectroscopy (EELS) appear at 504 and 653 cm^{-1}, respectively.[19] The vibrational mode at 630 cm^{-1} for $Ti_{14}C_{13}$ is assumed to correspond to the vibrational modes parallel to the TiC surface.[3,19]

The calculated IR spectra for the TiC nanocrystals consist largely of three strong bands at about 500, 600, and 700 cm^{-1}. For nanoclusters larger than $Ti_{32}C_{32}$, the bands at 500 and 600 cm^{-1} most likely unite to one single peak approaching the vibrational transition spectrum of bulk TiC. Surprisingly, for

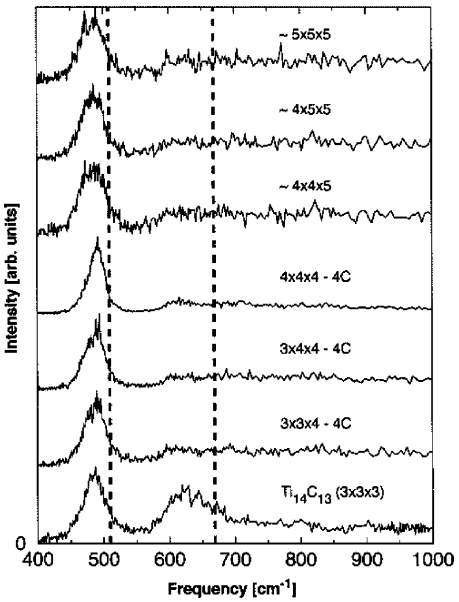

Figure 5. Measured IR-REMPI spectra of different nanocrystalline titanium carbide clusters. The two optically active surface phonon modes of bulk TiC are shown as the dashed lines.[19] Reprinted with permission from ref 3. Copyright 2003 American Chemical Society.

larger TiC clusters, the 630 cm^{-1} peak in the IR-REMPI spectra in Figure 5 is found to be very weak, and for the largest TiC nanocrystals, it even disappears into an almost constant background. Instead, one would expect a continuous transition from a molecular spectrum with distinct vibrational frequencies to a vibrational spectrum that is more or less reminiscent of the vibrational spectrum of the (100) surface of bulk TiC with peaks at 504 and 653 cm^{-1}.

The vibrational modes of $Ti_{32}C_{32}$ in the interval 130−200 cm^{-1} consist of skewing and breathing motions of the crystallite. Titanium motions dominate in the range 200−450 cm^{-1}, and the vibrational modes above 450 cm^{-1} involve mainly the carbon atoms. The transition at 533 cm^{-1} can be described as a breathing mode of the carbon lattice. The mode at 597 cm^{-1} is a triply degenerate stretching mode of the carbon lattice toward the carbon vertices, and the mode at 613 cm^{-1} is a similar motion but toward the titanium vertices. These two modes are related to the out-of-plane vibrational motion of solid TiC, whereas the modes at 709 and 724 cm^{-1} are the symmetric and asymmetric carbon motions related to the in-plane vibrational mode of solid TiC.

For Ti_4C_4, the vibrational mode at 351 cm^{-1} is a triply degenerate stretching mode of the Ti tetrahedron, whereas the modes at 663 and 718 cm^{-1} seem to be related to the out-of-plane mode and to the in-plane mode of solid TiC, respectively.

The triply degenerate strong low-energy vibration of $Ti_{14}C_{13}$ at 275 cm^{-1} consists of back and forward movements of the four titanium atoms in the middle plane and of the central carbon. The motion of the central plane pushes out the carbon atoms at the edge. The motion of the vibrational mode at 486 cm^{-1} is very similar, but for this mode, the central carbon atom is not involved. The vibration at 514 cm^{-1} can be characterized as an out-of-plane mode of the carbon atoms, whereas the ones at 670 and 673 cm^{-1} are related to the in-plane motions of the carbon atoms in solid TiC.

In the calculated IR spectrum of $Ti_{14}C_{13}$, one strong vibrational mode appears at 275 cm^{-1}, whereas, in the IR-REMPI measurement, no peaks have been detected in this energy region. Either this strong IR peak is due to computational difficulties or, alternatively, it cannot been observed in the IR-REMPI experiment. Vibrational modes with large anharmonicities can become very weak bands in the RI-REMPI spectrum, or the band might even be absent.[3] One has to bear in mind that in IR-REMPI spectroscopy the electron emission process has to compete with many cooling mechanisms and the intensities can therefore differ significantly from those obtained in ordinary absorption spectroscopy measurements.

The nanocrystals with an equal number of Ti and C atoms are also found to have vibrational transitions below 500 cm^{-1}. However, since the intensities of these modes are small, they can hardly be detected using any experimental technique to measure the IR spectra. For all TiC clusters considered, strong vibrational bands appear at wavenumbers between 600 and 800 cm^{-1}, whereas, in the IR-REMPI measurement on large TiC nanocrystals such as $Ti_{18}C_{18}$ and $Ti_{32}C_{32}$, the intensity of this band is vanishingly small.

V. Optical Gaps

$Ti_{14}C_{13}$ and $Ti_{63}C_{62}$ are nanocrystals with nonstoichiometric TiC compositions which might introduce some computational complications; they are most likely multiconfiguration cases. This means that present-day DFT functionals have difficulties in describing them accurately. For $Ti_{14}C_{13}$ and $Ti_{63}C_{62}$, the HOMO−LUMO splittings calculated at the BP DFT/TZVP level are only 0.060 eV (484 cm^{-1}) and 0.0068 eV (55 cm^{-1}), respectively. For the TiC nanoclusters with an equal number of Ti and C atoms such as Ti_4C_4, $Ti_{18}C_{18}$, and $Ti_{32}C_{32}$, the energy gap between the highest occupied molecular orbital (HOMO) and the lowest unoccupied molecular orbital (LUMO) calculated at the BP DFT/TZVP level are 2.27, 0.42, and 0.55 eV. The corresponding HOMO−LUMO gaps calculated at the PBE0 DFT/TZVP level are 4.10, 1.77, and 1.74 eV. For $Ti_{108}C_{108}$, the HOMO−LUMO gap obtained at the BP DFT/SVP and PBE0 DFT/SVP levels are 0.027 and 0.32 eV, respectively. The nanoclusters with an equal number of Ti and C atoms have thus larger HOMO−LUMO splittings than the one-step smaller ones with an odd number of atoms, even though the HOMO−LUMO gap is expected to decrease with increasing size of the nanocrystals, approaching metallic bulk TiC with zero gap.

The first singlet excitation energies of 2.41, 1.27, 0.248, 0.918, 0.615, 0.011, and 0.028 eV for Ti_4C_4, $Ti_{12}C_{12}$, $Ti_{14}C_{13}$, $Ti_{18}C_{18}$, $Ti_{32}C_{32}$, $Ti_{63}C_{62}$, and $Ti_{108}C_{108}$, respectively, calculated at the BP DFT level using the TDDFT approach are slightly larger than the HOMO−LUMO gaps given in Table 1. In the TDDFT calculations on the largest TiC nanoclusters, the SVP quality basis sets were employed. The excitation energy of the first excited state of $Ti_{32}C_{32}$ calculated at the BP DFT/SVP level is only 4% smaller than the corresponding value obtained using the TZVP basis sets. Thus, a TZVP calculation on $Ti_{108}C_{108}$ would yield qualitatively the same excitation energy of the first excited state as that obtained with the smaller basis set.

The calculation of the first few triplet excitation energies for $Ti_{108}C_{108}$ showed that the lowest triplet state is practically degenerate with the lowest singlet state. The optical gap of 0.028 eV for $Ti_{108}C_{108}$ calculated at the BP DFT/SVP level corresponds to a temperature of 325 K. Thus, according to the BP TDDFT calculations, the occupation of the first excited state at room temperature is 34% and the low-lying discrete states would be observed experimentally as a broad and unstructured IR-REMPI spectrum.[3] However, the HOMO−LUMO gap of $Ti_{108}C_{108}$ calculated at the PBE0 DFT level is 0.32 eV, showing that the largest nanocluster considered here is still nonmetallic with a significant optical gap.

Even though TiC is metallic in the bulk, the present nanocrystals are nonmetallic. The low-lying excited states of the nanocrystals form discrete states just above the Fermi level, whereas the band with a large density of states (DOS) is still well-separated from the Fermi level. For the largest clusters, the discrete states approach the Fermi level and the band also expands toward longer wavelengths. For $Ti_{32}C_{32}$, the HOMO−LUMO gap calculated at the BP DFT/TZVP level is 0.55 eV and the band structure begins to appear at about 1.5 eV above the Fermi level. By comparison, Ti_4C_4 has at the BP DFT/TZVP level a HOMO−LUMO gap of 2.27 eV and its band with a large DOS lies above 8 eV. This is probably how the transition from nonmetallic nanocrystals to a solid-state metallic material occurs.

VI. Conclusions

In this paper, we have demonstrated the possibility of calculating IR absorption spectra for large TiC nanocrystals. The calculated spectra are compared to vibrational spectra obtained using the infrared resonance-enhanced multiphoton ionization (IR-REMPI) experimental technique.[3] The calculated and measured spectra largely agree, but some significant discrepancies are also obtained. For $Ti_{32}C_{32}$, three strong bands are calculated at 533, 597, and 709 cm^{-1}, respectively, whereas the experimental spectrum shows only one strong band at 450−500 cm^{-1}. The band at 600−700 cm^{-1} detected for $Ti_{14}C_{13}$ becomes very weak for the larger TiC nanocrystals, and for the largest ones, it even disappears into the background noise (see Figure 5), whereas, according to the calculations, the strong vibrational modes at 600−700 cm^{-1} are present also in the larger nanocrystals even though they are not observed in the IR-REMPI measurement. The notion that the vibrational properties of $Ti_{14}C_{13}$ ($3 \times 3 \times 3$) are very close to those of bulk TiC and bridging the gap between TiC nanocrystals and bulk is not quite correct; the agreement between the energy of the vibrational bands of $Ti_{14}C_{13}$ obtained using IR-REMPI spectroscopy and the vibrational energies of bulk TiC seems to be fortuitous. All nanocrystals studied in this work are found to be nonmetallic; the HOMO−LUMO gap of the largest TiC nanocrystal, that is, of $Ti_{108}C_{108}$ ($6 \times 6 \times 6$) is calculated at the PBE0 DFT/SVP level to be 0.32 eV. For the largest nanocrystals, the first signs of the transition from nonmetallic nanocrystals to a metallic conductor become apparent.

Acknowledgment. We acknowledge financial support from the European research training network on "Understanding Nanomaterials from a Quantum Perspective" (NANOQUANT), Contract No. MRTN-CT-2003-506842, from the Nordisk Forskerakademi network for research and research training (NorFA Grant No. 030262) on "Quantum Modeling of Molecular Materials" (QMMM), from The Academy of Finland (FA projects 53915, 200903, and 206102), and from Magnus Ehrnrooth's Foundation. We also thank Prof. Reinhart Ahlrichs (Karlsruhe) for an up-to-date version of the TURBOMOLE program package and CSC—Scientific Computing Ltd. for computer time.

References and Notes

(1) Guo, B. C.; Kerns, K. P.; Castleman, A. W., Jr. *Science* **1992**, *255*, 1411.
(2) Pilgrim, J. S.; Duncan, M. A. *J. Am. Chem. Soc.* **1993**, *115*, 9724.
(3) von Helden, G.; van Heijnsbergen, D.; Meijer, G. *J. Phys. Chem. A* **2003**, *107*, 1671.
(4) Rohmer, M. M.; Bénard, M.; Poblet, J. M. *Chem. Rev.* **2000**, *100*, 495.
(5) Zhang, Q.; Lewis, S. P. *Chem. Phys. Lett.* **2003**, *372*, 836.
(6) von Helden, G.; van Heijnsbergen, D.; Duncan, M. A.; Meijer, G. *Chem. Phys. Lett.* **2001**, *333*, 350.
(7) van Heijnsbergen, D.; von Helden, G.; Duncan, M. A.; van Roij, A. J. A.; Meijer, G. *Phys. Rev. Lett.* **1999**, *83*, 4983.
(8) von Helden, G.; Tielens, A. G. G. M.; van Heijnsbergen, D.; Duncan, M. A.; Hony, S.; Waters, L. B. F. M.; Meijer, G. *Science* **2000**, *288*, 313.
(9) van Heijnsbergen, D.; Duncan, M. A.; Meijer, G.; von Helden, G. *Chem. Phys. Lett.* **2001**, *349*, 220.
(10) van Heijnsbergen, D.; Fielicke, A.; Meijer, G.; von Helden, G. *Phys. Rev. Lett.* **2002**, *89*, 013401.
(11) Selvan, R.; Pradeep, T. *Chem. Phys. Lett.* **1999**, *309*, 149.
(12) Gueorguiev, G. K.; Pacheco, J. M. *Phys. Rev. B* **2003**, *68*, 241401.
(13) Gueorguiev, G. K.; Pacheco, J. M. *Phys. Rev. Lett.* **2002**, *88*, 115504.
(14) Baruah, T.; Pederson, M. R.; Lyn, M. L.; Castleman, A. W., Jr. *Phys. Rev. A* **2002**, *66*, 053201.
(15) Baruah, T.; Pederson, M. R. *Phys. Rev. B* **2002**, *66*, 241404.
(16) Hou, H.; Muckerman, J. T.; Liu, P.; Rodrigues, J. A. *J. Phys. Chem. A* **2003**, *107*, 9344.
(17) Liu, P.; Rodriguez, J. A.; Hou, H.; Muckerman, J. T. *J. Chem. Phys.* **2003**, *118*, 7737.
(18) Postnikov, A. V.; Entel, P. *Phase Transitions* **2004**, *77*, 149.
(19) Oshima, C.; Aizawa, T.; Wuttig, M.; Souda, R.; Otani, S.; Ishizawa, Y.; Ishida, H.; Terakura, K. *Phys. Rev. B* **1987**, *36*, 7510.
(20) Eichkorn, K.; Treutler, O.; Öhm, H.; Häser, M.; Ahlrichs, R. *Chem. Phys. Lett.* **1995**, *240*, 283.
(21) Vosko, S. H.; Wilk, L.; Nusair, M. *Can. J. Phys.* **1980**, *58*, 1200.
(22) Perdew, J. P. *Phys. Rev. B* **1986**, *33*, 8822.
(23) Becke, A. D. *Phys. Rev. A* **1988**, *38*, 3098.
(24) Ahlrichs, R.; Bär, M.; Häser, M.; Horn, H.; Kölmel, C. *Chem. Phys. Lett.* **1989**, *162*, 165 (for current version, see http://www.turbomole.de).
(25) Schäfer, A.; Huber, C.; Ahlrichs, R. *J. Chem. Phys.* **1994**, *100*, 5829.
(26) http://www.turbomole.de/.
(27) Bauernschmitt, R.; Ahlrichs, R. *Chem. Phys. Lett.* **1996**, *256*, 454.
(28) Bauernschmitt, R.; Häser, M.; Treutler, O.; Ahlrichs, R. *Chem. Phys. Lett.* **1997**, *264*, 573.
(29) Furche, F.; Ahlrichs, R. *J. Chem. Phys.* **2002**, *117*, 7433.
(30) Schäfer, A.; Horn, H.; Ahlrichs, R. *J. Chem. Phys.* **1992**, *97*, 2571.
(31) Perdew, J. P.; Burke, K.; Ernzerhof, M. *Phys. Rev. Lett.* **1996**, *77*, 3865.
(32) Toth, L. E. *Transition Metal Carbides and Nitrides*; Academic Press: New York, 1971.
(33) Barret, C. S.; Massalski, T. B. *Structure of Metals: Crystallographic Methods, Principles, and Data*; Pergamon Press: New York, 1980.